JACS
JOURNAL OF THE AMERICAN CHEMICAL SOCIETY
Article
pubs.acs.org/JACS

Bithiopheneimide−Dithienosilole/Dithienogermole Copolymers for Efficient Solar Cells: Information from Structure−Property−Device Performance Correlations and Comparison to Thieno[3,4-*c*]pyrrole-4,6-dione Analogues

Xugang Guo,[†,▽] Nanjia Zhou,[‡,▽] Sylvia J. Lou,[†] Jonathan W. Hennek,[†] Rocío Ponce Ortiz,[†,§] Melanie R. Butler,[†] Pierre-Luc T. Boudreault,[†] Joseph Strzalka,[∥] Pierre-Olivier Morin,[¶] Mario Leclerc,[¶] Juan T. López Navarrete,[§] Mark A. Ratner,*[,†] Lin X. Chen,*[,†] Robert P. H. Chang,*[,‡] Antonio Facchetti,*[,†,‡,⊥] and Tobin J. Marks*[,†,‡]

[†]Department of Chemistry and the Materials Research Center, the Argonne-Northwestern Solar Energy Research Center, Northwestern University, 2145 Sheridan Road, Evanston, Illinois 60208, United States

[‡]Department of Materials Science and Engineering and the Materials Research Center, the Argonne-Northwestern Solar Energy Research Center, Northwestern University, 2145 Sheridan Road, Evanston, Illinois 60208, United States

[§]Department of Physical Chemistry, University of Málaga, Campus de Teatinos s/n, Málaga 29071, Spain

[∥]X-ray Science Division, Argonne National Laboratory, Argonne, Illinois 60439, United States

[¶]Département de Chimie, Université Laval, Quebec City, Quebec G1V 0A6, Canada

[⊥]Polyera Corporation, 8045 Lamon Avenue, Skokie, Illinois 60077, United States

Supporting Information

ABSTRACT: Rational creation of polymeric semiconductors from novel building blocks is critical to polymer solar cell (PSC) development. We report a new series of bithiopheneimide-based donor−acceptor copolymers for bulk-heterojunction (BHJ) PSCs. The bithiopheneimide electron-deficiency compresses polymer bandgaps and lowers the HOMOs—essential to maximize power conversion efficiency (PCE). While the dithiophene bridge progression $R_2Si \rightarrow R_2Ge$ minimally impacts bandgaps, it substantially alters the HOMO energies. Furthermore, imide *N*-substituent variation has negligible impact on polymer opto-electrical properties, but greatly affects solubility and microstructure. Grazing incidence wide-angle X-ray scattering (GIWAXS) indicates that branched *N*-alkyl substituents increased polymer $\pi-\pi$ spacings vs linear *N*-alkyl substituents, and the dithienosilole-based **PBTISi** series exhibits more ordered packing than the dithienogermole-based **PBTIGe** analogues. Further insights into structure−property−device performance correlations are provided by a thieno[3,4-*c*]pyrrole-4,6-dione (**TPD**)−dithienosilole copolymer **PTPDSi**. DFT computation and optical spectroscopy show that the **TPD**-based polymers achieve greater subunit−subunit coplanarity via intramolecular (thienyl)S···O(carbonyl) interactions, and GIWAXS indicates that **PBTISi-C8** has lower lamellar ordering, but closer $\pi-\pi$ spacing than does the **TPD**-based analogue. Inverted BHJ solar cells using bithiopheneimide-based polymer as donor and $PC_{71}BM$ as acceptor exhibit promising device performance with PCEs up to 6.41% and $V_{oc} > 0.80$ V. In analogous cells, the **TPD** analogue exhibits 0.08 V higher V_{oc} with an enhanced PCE of 6.83%, mainly attributable to the lower-lying HOMO induced by the higher imide group density. These results demonstrate the potential of **BTI**-based polymers for high-performance solar cells, and provide generalizable insights into structure−property relationships in **TPD**, **BTI**, and related polymer semiconductors.

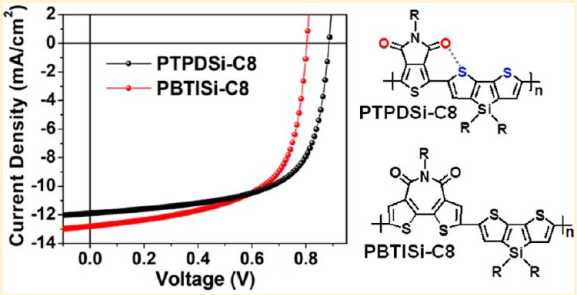

INTRODUCTION

Polymer solar cells (PSCs) have recently received great attention as renewable energy sources because of their compatibility with fabricating large-area, flexible, and cost-effective devices via roll-to-roll (R2R) processing techniques.[1,2] Moreover, solar cell power conversion efficiencies (PCEs) have increased substantially over the past few years as a consequence of improved active layer materials,[3,4] film morphology optimization,[5] interface engineering,[6,7] and improved device architectures.[8−10] Impressive PCEs surpassing 8%[6c,9b,10,11] have been achieved with PSC active regions configured in a bulk-heterojunction (BHJ) network of intermingled π-conjugated polymer electron donors and high electron-affinity fullerene electron acceptors.[12−15]

Received: August 16, 2012
Published: October 3, 2012

 © 2012 American Chemical Society

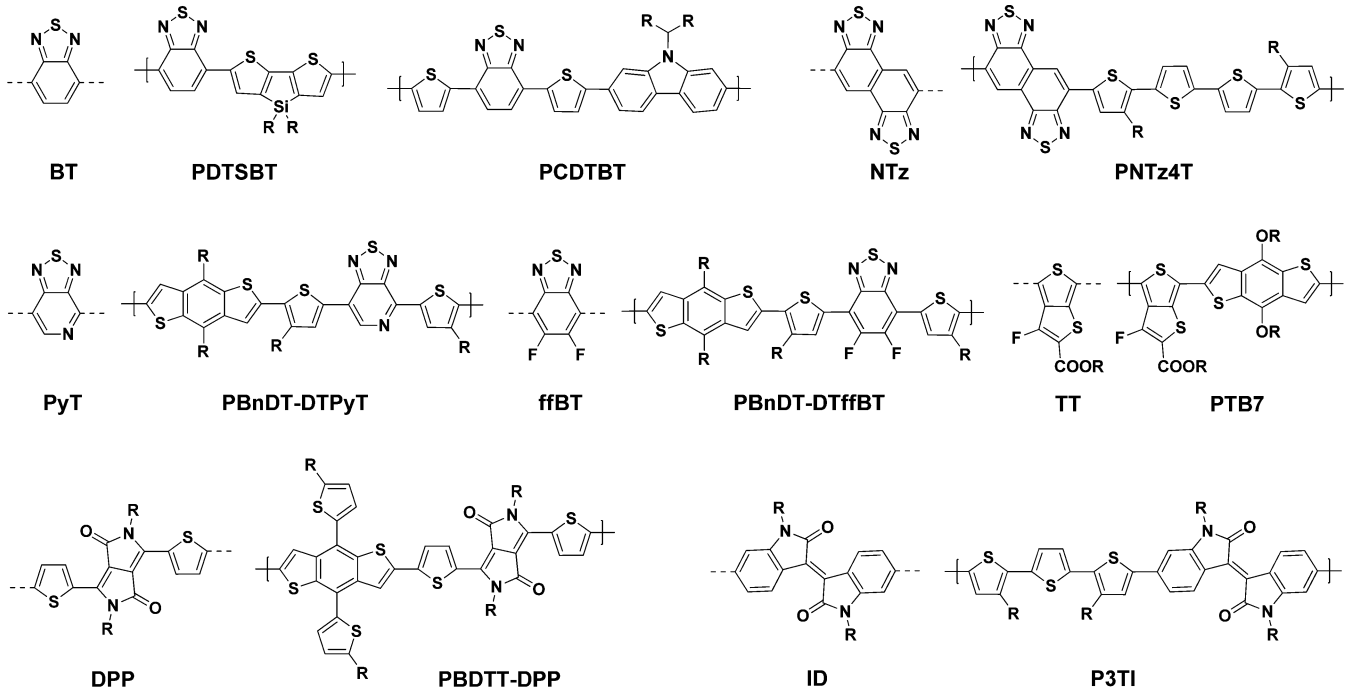

Figure 1. Chemical structures of effective acceptor units and representative donor−acceptor copolymers for high-performance polymer solar cells constructed from these acceptor units.

The development of more effective donor polymers with appropriate bandgaps and frontier molecular orbital (FMO) energy levels[16] remains a major challenge for next-generation PSCs.[3,15] Among various donors used in BHJ solar cells, the most promising ones are conjugated in-chain donor−acceptor (D-A) copolymers, which consist of alternating donor and acceptor blocks in each repeating unit.[3b,12b,15] The D−A strategy not only allows effective tuning of the bandgap, but also tailoring of the resultant polymer FMO energies.[3b,16] Low bandgaps can maximize absorption of the solar flux, while appropriate FMO energies should enhance exciton dissociation efficiency at the BHJ donor/acceptor interface while promoting high open-circuit voltages (V_{oc}'s) to maximize overall performance.[13,14] The design, synthesis, and incorporation of appropriate acceptor units is a critical factor in developing high-performance D−A polymers. Although both the donor and acceptor units make contributions to the FMO energies in such copolymers through orbital hybridization,[3b,16a] the lowest unoccupied molecular orbital (LUMO) and the highest occupied molecular orbital (HOMO) are mainly localized on the acceptor and donor co-units, respectively. Thus, the LUMO positions not only influence the bandgap, but also affect the exciton dissociation efficiency at the polymer donor/fullerene acceptor interfaces.

In comparison to the great advances in donor (D) blocks of the repeating units in D−A polymers, the availability of effective acceptor (A) moieties has been severely limited. Among the few effective A blocks, the 2,1,3-benzothiadiazole group (**BT**, Figure 1) has been heavily investigated and a large number of **BT**-based copolymers have been reported.[17] For example, PCEs of 5.9% has been obtained from benzothiadiazole−dithienosilole copolymers (**PDTSBT**) with exceptionally high J_{sc} values of 17.3 mA/cm^2.[17e] Note that the PCEs of the **PDTSBT**-based polymers are limited by the small V_{oc} of 0.57 V.

However, by inserting two flanking thiophene spacers and using carbazole donor co-units, impressive device performance with a significantly higher V_{oc} of 0.88 V and a PCE of 6.1% is achieved in optimized **PCDTBT**-based PSCs.[17f] Although the low-lying **PCDTBT** HOMO affords a sizable V_{oc}, these polymers are limited by the large bandgaps (∼1.9 eV) caused by the high-lying LUMOs (−3.6 eV).[18] Indeed, among the great many **BT**-based BHJ systems, few exhibit PCEs greater than 6%, mainly due to high-lying HOMOs or large bandgaps. In order to depress the polymer LUMOs, naphthobisthiadiazole (**NTz**, Figure 1),[19a] a doubly benzothiadiazole-fused heterocyle, has been incorporated into polymer backbones, and the resultant polymer, **PNTz4T**, features a lower LUMO (−3.77 eV) than does the benzothiadiazole analogue (−3.53 eV). As a result, **PNTz4T**-based BHJ PSCs achieve a V_{oc} of ∼0.75 V, J_{sc} of 12 mA/cm^2, and a PCE of 6.3%.[19b] Other benzothiadiazole derivatives having electron deficiency greater than that of **BT** have also been incorporated into PSC materials, such as pyridalthiadiazole (**PyT**)[18] and fluorinated benzothiadiazole (**ffBT**), and the resultant polymers, **PBnDT-DTPyT**[20] and **PBnDT-DTffBT** (Figure 1),[4b] exhibit promising performance with PCEs of 6−7%. As one of most important acceptor units in organic electronics, 1,4-diketopyrrolopyrrole (**DPP**, Figure 1) has been incorporated into PSC polymer backbones, beginning with Janssen's **DPP**-based polymer PSCs.[21a] Such materials typically have small bandgaps due to the electron-withdrawing lactam rings, and BHJ devices exhibit PCEs of 4−5% when combined with various electron-donating co-units;[3f,21b,c] a PCE of 6.5% was recently achieved in **PBDTT-DPP**-based PSCs.[21d] The factor limiting **DPP**-based BHJ device performance appears to be the high-lying HOMO levels, reflecting the **DPP**-flanking thiophenes which dilute the lactam ring density in the backbone. Isoindigo (**ID**),[22] another lactam-functionalized acceptor, also shows potential for constructing low bandgap PSC polymers, with **P3TI** (Figure 1) exhibiting a PCE of 6.3% but a V_{oc} of only 0.70 V.[22c] Using ester-functionalized thieno[3,4-*b*]thiophene (**TT**, Figure 1) as the acceptor unit, Yu developed a series of **PTBx** polymers (x = 1−6) by copolymerizing ester-functionalized **TT** units with benzodithiophene. The electron-with-

drawing ester groups together with the **TT** tendency to stabilize quinoidal structures affords polymers with bandgaps of ∼1.6 eV. Functionalizing the acceptor unit with fluorine lowers the HOMO and LUMO energies further, and BHJ devices using **PTB7** (Figure 1) achieved PCE >7% for the first time.[23] To date, ester-functionalized **TT**s have been one of the most important acceptor units for constructing high-performance photovoltaic polymers.[3e]

Imide-functionalized arenes (Figure 2)[3f,24,25] are attractive BHJ polymer acceptor units due to their compatibility with solubilizing substituents, electron-deficient characteristics, and structure-enforcing geometries, which can synergistically integrate desirable opto-electronic properties into a single macromolecular architecture (Figure 2a). Note first that the strong imide group electron-withdrawing capacity enables tuning of the copolymer bandgap and FMO energies,[3f,26] of primary concern[13] for optimizing solar cell performance among others, such as carrier mobility,[3b,15b] dipole moment,[27] and film morphology.[5] Second, π-conjugated (macro)molecules are typically synthesized using Pd-mediated coupling reactions,[28] and the dibrominated imide monomer electron deficiency favors efficient Pd(0) catalyst C−Br oxidative addition and subsequent coupling with electron-rich comonomers, to yield high molecular weight copolymers,[26,29] an asset for PSC performance.[17e,30] Third, facile imide backbone *N*-alkylation enables manipulation of polymer solubility and solid-state packing without disrupting close π−π stacking required for efficient carrier transport,[29,31] and intermolecular donor−acceptor interactions can promote close intermolecular π-orbital overlap. Furthermore, the solubilizing/crystallizing tendencies of imide *N*-substituents should facilitate fine-tuning of materials structural organization to optimize PSC performance.[32] Lastly, S···O interactions involving proximate imide C═O groups and thienyl S atoms (see Figure 6c as an example) can serve as conformational "locks" to enhance π-system coplanarity.[33] In comparison to **BT** and its derivatives **PyT**, **ffBT**, and **NTz** (Figure 1), imide-functionalized arenes can enhance polymer solubility and offer stronger electron-withdrawing capacities than lactam or amide fragments, thereby yielding smaller bandgaps and lower-lying LUMOs than **DPP**- or **ID**-based polymers.

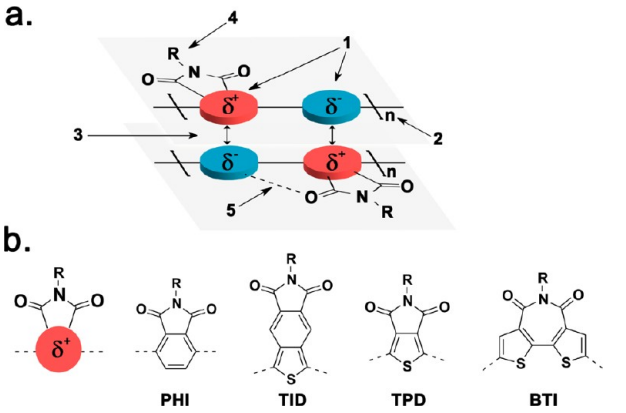

Figure 2. (a) Imide-functionalized donor−acceptor (D−A) copolymers combining performance-enhancing properties for solar cell applications. (1) D−A strategy for bandgap and frontier MO energy tuning. (2) High molecular weights. (3) Close π−π stacking. (4) Solubility and crystallinity via imide *N*-alkylation. (5) Conformational locking to promote π-system coplanarity via (thienyl)S···O(carbonyl) interactions. (b) Representative imide-functionalized arenes as electron-deficient units for D−A solar cell copolymers.

Among various imide-functionalized polymers, phthalimide (**PHI**, Figure 2)-based polymer semiconductors were first reported by Watson[29] and show promising PCEs of 2−4% in PSCs.[24] Due to the large resonance energy of benzene (1.56 eV), which limits the quinoidal character of **PHI**-based polymers, highly electron-rich dialkoxybithiophenes must be used as donor co-units in order to narrow the bandgap (<1.70 eV), which results in low PSC V_{oc}'s (<0.6 V).[24] Thienoisoindoledione (**TID**, Figure 2),[25a] an imide-functionalized bicyclic compound containing a benzene ring fused to the C3−C4 positions of thiophene, can achieve narrow bandgaps through competing aromaticity between the arene and thiophene groups. The greater resonance energy of the arene vs that of thiophene (1.26 eV) favors increased aromaticity of the arene portion, imparting significant quinoidal character to **TID**-based polymers and narrowing the bandgaps.[25] Despite the optimized bandgaps, **TID**-based polymers usually exhibit low PCEs (≤3%), presumably due to inefficient exciton dissociation induced by the deep LUMOs and low carrier mobilities due to the backbone torsion created by the sterically active hydrogen atom on the **TID** isoindole fragment.[25b] In comparison to **PHI**, thieno[3,4-*c*]pyrrole-4,6-dione (**TPD**, Figure 2) should be a more promising acceptor moiety due to its geometry and smaller aromatic resonance energy and geometry, which should decrease steric hindrance and promote quinoidal character, respectively, to achieve favorable properties such as high backbone coplanarity, enhanced electron delocalization, and low bandgaps.[34] The unique properties make **TPD**-based polymers one of most successful materials families for implementation in PSCs.[3f] As an emerging building block, bithiopheneimide (**BTI**, Figure 2)-based polymer semiconductors have achieved promising device performance in organic thin-film transistors (OTFTs), with electron and hole mobilities surpassing 0.1 $cm^2/(V\ s)$ for **PBTimR** and **PBTI4T**, respectively (Figure 3).[35] Beyond very good charge transport, **BTI**-based p-type polymers exhibit excellent OTFT air stability due to the low-lying HOMOs. The broad optical absorption spectra, low-lying HOMOs, good solubilities, and promising charge transport properties of **BTI**-

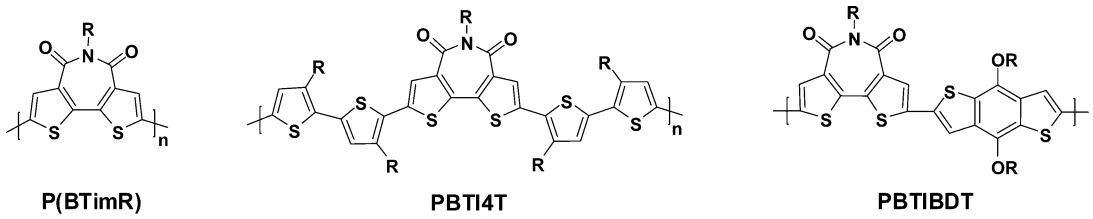

Figure 3. Structures of bithiopheneimide-based polymers for high-performance organic electronics: **P(BTimR)** n-type and **PBTI4T** p-type semiconductors for organic thin-film transistors, and **PBTIBDT** as an active-layer electron donor component for BHJ polymer solar cells.

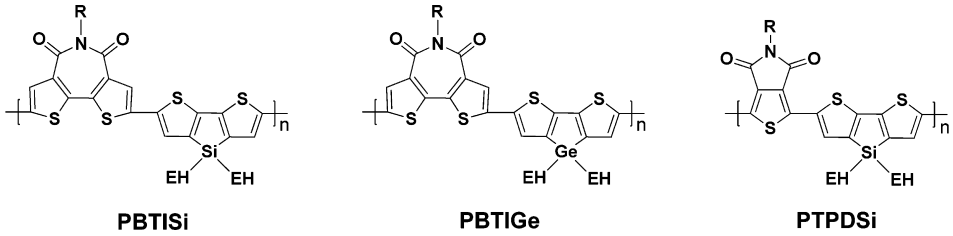

Figure 4. Structures of bithiopheneimide and dithienosilole copolymers (**PBTISi**) and bithiopheneimide and dithienogermole (**PBTIGe**) copolymers for efficient polymer solar cells. Thieno[3,4-*c*]pyrrole-4,6-dione and dithienosilole copolymer (**PTPDSi**)[38c] were synthesized for comparison. EH = 2-ethylhexyl.

Scheme 1. Synthetic Route to BTI Monomers and BTI-Based Copolymers PBTISi and PBTIGe[a]

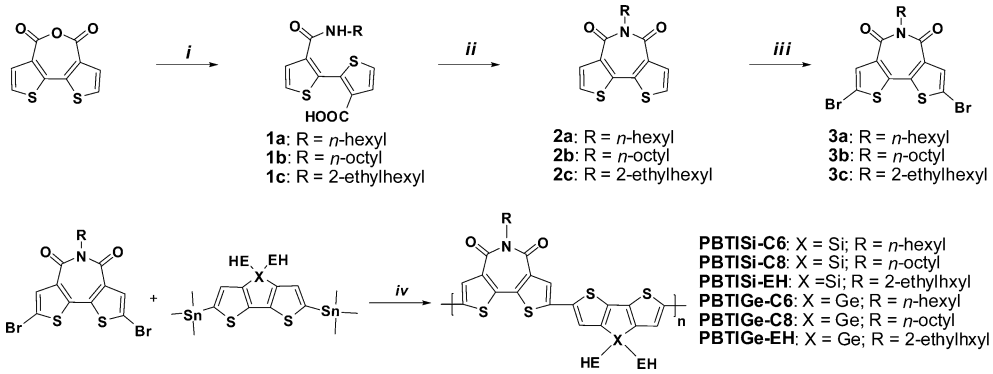

[a]Reagent and conditions: (*i*) RNH_2, DCM, reflux; (*ii*) $SOCl_2$, reflux; (*iii*) Br_2, $FeCl_3$, DCM; (*iv*) $Pd_2(dba)_3$, P(*o*-tolyl)$_3$, toluene, 110 °C (EH = 2-ethylhexyl).

based polymers inspired us to modify their chemical structures for solar cell applications. In initial studies, we investigated **BTI** copolymerizations with electron-rich benzodithiophenes (**BDTs**)[36] and recently reported bithiopheneimide and benzodithiophene copolymers **PBTIBDT** (Figure 3) with promising PCEs of 5.5%, as well as large open-circuit voltages (V_{oc}'s) greater than 0.9 V.[37] The bottleneck for optimal performance here appears to be the relatively large bandgaps (~1.95 eV) due to unfavorable quinoidal character, which limits exciton formation. Recently the dithienosilole (**DTS**)[38] and dithienogermole (**DTG**)[9] fragments have been proposed as electron-rich co-units for constructing low bandgap polymers while achieving low-lying HOMOs to maximize short-circuit current (J_{sc}) without sacrificing V_{oc}. In the present contribution, we investigate the copolymerization of **DTS** and **DTG** comonomers with **BTI** units to afford **BTI**−dithienosilole (**PBTISi**, Figure 4) and **BTI**−dithienogermole (**PBTIGe**) copolymers having low bandgaps (~1.75 eV) for PCS applications. We also probe the effects of the bridging group 14 heteroatom identity on the polymer structural and opto-electronic properties, and on the PSC performance. By further modifying the imide *N*-side chains, we also investigate substituent effects on the film microstructure. It will be seen that the branched *N*-substituent, 2-ethylhexyl, slightly increases the intermolecular $\pi-\pi$ spacing, and therefore diminishes the charge transport capacity, leading to smaller J_{sc}'s and fill factors (FFs) in **PBTISi-EH** and **PBTIGe-EH**-based PSCs. Optimizing the side chains and device fabrication conditions affords PCEs as high as 6.41% with V_{oc}'s exceeding 0.8 V in inverted **PBTISi-C8**-based BHJ cells, thus indicating the potential of **BTI**-based copolymers for organic solar cells. Furthermore, to better understand structure−property device performance relationships in **BTI**-based polymers, the state-of-the-art performance thieno[3,4-*c*]-4,6-dione-dithienosilole copolymer (**PTPDSi-C8**, R = *n*-octyl, Figure 4)[30,38c] was synthesized to compare with **PBTISi-C8**. It will be seen that **PTPDSi-C8** has a higher degree of conjugation enforced by the planarizing intramolecular (thienyl)S···O(carbonyl) interaction,[33] therefore a smaller bandgap and superior transport properties to **PBTISi-C8**. Thus, **PTPDSi-C8**-based PSCs exhibit a larger V_{oc} of 0.885 V and a higher PCE of 6.83%, reflecting the lower-lying HOMO, due in turn to the higher imide group density in the polymer backbone vs **PBTISi-C8**.

■ RESULTS AND DISCUSSION

Synthesis of BTI-Based Monomers and Polymers. The general synthesis of the key intermediate, bithiopheneimide, **2** (Scheme 1), was reported previously from this laboratory.[31] Starting from bithiophene anhydride, microwave-assisted imidization leads to the **BTI**, **2**, products in moderate yields (30−70%), depending on the *N*-functionalization. Branched amines usually afford lower yields than do linear amines.[31] The modified procedure of Scheme 1 greatly improves the reaction yields. In particular, slow addition of the amine in dichloromethane to the bithiophene anhydride in dichloromethane solution under reflux affords carbamoyl intermediates **1**, which are purified by flash column chromatography using ethyl acetate as eluent (see Supporting Information) to remove unreacted starting materials. The carbamoyl derivatives are then subjected to thionylchloride-assisted imidization, which produces **2** in much higher yields, typically with overall two-step yields exceeding 80%, even for highly encumbered amines, such as 2-hexyldecyl amine. Subsequent dibromination of imides **2** provides monomers **3** in quantitative yield (>95%). Next, the distannylated dithienosilole[38a] and dithienogermole[9a] monomers are synthesized according to published procedures. After

Table 1. Molecular Weight, Optical and Electrochemical Properties of BTI-Based Polymers PBTISi and PBTIGe and TPD-based polymer PTPDSi-C8

polymer	M_n (kDa)[a]	PDI[a]	λ_{max} soln (nm)[b]	$\lambda_{shoulder}$ abs soln (nm)[b]	λ_{max} abs film (nm)[c]	$\lambda_{shoulder}$ abs film (nm)[c]	E_{HOMO} (eV)[d]	E_{LUMO} (eV)[e]	E_g^{opt} (eV)[f]
PBTISi-C6	29	3.3	603	640	590	637	−5.45	−3.70	1.75
PBTISi-C8	30	3.1	603	639	592	637	−5.43	−3.68	1.75
PBTISi-EH	26	2.8	597	633	588	633	−5.42	−3.65	1.77
PBTIGe-C6	27	2.9	607	642	593	641	−5.39	−3.64	1.75
PBTIGe-C8	25	2.7	607	641	591	637	−5.38	−3.63	1.75
PBTIGe-EH	18	2.3	598	634	590	635	−5.38	−3.62	1.76
PTPDSi-C8	29	1.8	673	616	671	611	−5.52	−3.79	1.73

[a]Determined by SEC at 170 °C in trichlorobenzene. [b]Solution absorption spectra (1×10^{-5} M in DCB). [c]Thin film absorption spectra from pristine film cast from 1 mg/mL DCB solution. [d]Electrochemically determined vs Fc/Fc^+; $E_{HOMO} = -(E_{ox}^{onset} + 4.80)$. [e]Calculated according to: $E_{LUMO} = E_g^{opt} + E_{HOMO}$. [f]Optical energy gap estimated from absorption edge of the as-cast thin film.

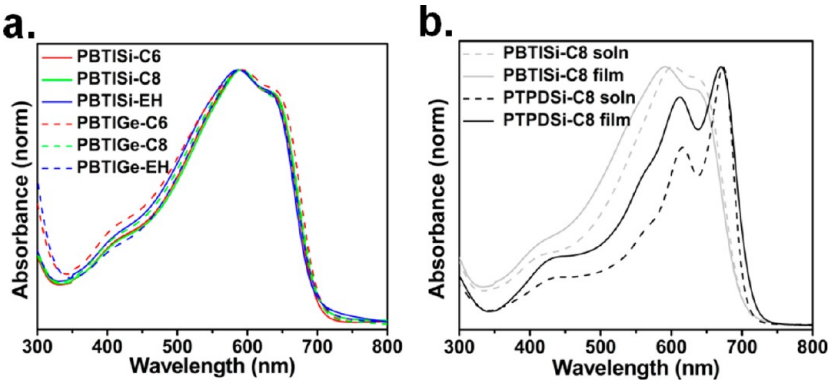

Figure 5. (a) Optical absorption spectra of bithiopheneimide copolymers as pristine films dropcast from DCB (1 mg/mL) and (b) optical absorption spectra of **PBTISi-C8** and **PTPDSi-C8** in DCB (1×10^{-5} M, based on the polymer repeat unit) and as pristine films dropcast from DCB (1 mg/mL).

workup, the ^{1}H and ^{13}C NMR spectra indicate high monomer purity (>98%). Further purification of the distannylated dithienosilole monomers can be accomplished by flash column chromatography using basic alumina as the stationary phase and hexane/triethylamine as eluent. Note that further purification of distannylated dithienogermole under these conditions leads to significant monomer decomposition. This inability to fully purify the distannylated dithienogermole may be a reason for the relatively low molecular weights obtained for the **PBTIGe** polymer series vs the corresponding **PBTISi** series. The synthesis of the **BTI**-based copolymers is carried out using Pd-mediated Stille polymerizations (Scheme 1). At this point, 2-trimethylstannylthiophene followed by 2-bromothiophene is added sequentially to end-cap the polymers. Finally, all polymeric products are purified by Soxhlet extraction using specific solvent sequences which depend on the polymer solubility characteristics. Size exclusion chromatography (SEC) measurements indicate that all of the new **BTI**-based polymers have M_n's greater than 18 kDa and a polydispersity index (PDI) of 2−3, with the **PBTISi** polymers typically having higher M_n's than the corresponding **PBTIGe** analogues (Table 1). The identity and purity of all the new **BTI** polymers are supported by ^{1}H NMR spectra and elemental analysis. All of these polymers have good solubility in chlorinated solvents (>10 mg/mL) at 25 °C, with **PBTISi-EH** and **PBTIGe-EH** having branched *N*-alkyl substituents exhibiting enhanced solubility vs those functionalized with linear groups, **PBTISi-C6**, **PBTSi-C8**, **PBTIGe-C6**, and **PBTIGe-C8**. No thermal transitions are detected for any of these polymers by DSC (Figure S1 in Supporting Information [SI]), suggesting amorphous or low crystallinity microstructures. **PTPDSi-C8** (Figure 4, R = *n*-octyl) is synthesized and purified by following a published procedure (SI), yielding an M_n of 29 kDa, comparable to that reported by Leclerc[38c] and Reynolds.[9a] In comparison to **PTPDSi-C8** having comparable M_n and identical solubilizing groups, **PBTISi-C8** exhibits excellent solubility although it contains a larger fused **BTI** unit.

Polymer Optical Properties. The optical properties of the **BTI**-based polymers were investigated by UV−vis absorption spectroscopy both as thin films (Figure 5) and in solution (Figure S3 in SI). Relevant data are summarized in Table 1. Figure 5a shows the absorption spectra of **BTI**-based polymers as thin films, with the absorption spectra of **PTPDSi-C8** both in solution and as a thin film provided for comparison to those of **PBTISi-C8** (Figure 5b). All of the **BTI**-based polymers exhibit strong absorption in the visible region with absorption maxima (λ_{max}) ranging from 588 to 607 nm and absorption shoulders ($\lambda_{shoulder}$) ranging from 633 to 642 nm in solution and as thin films. From the absorption spectra, it can be seen that there are no significant bathochromic shifts on going from solution to the solid state (Figures 5 and S3 [SI]), suggesting that strong aggregation of these polymers in solution is promoted by the planar fused π-electron structures and attractive intermolecular donor/acceptor interactions. Variation of imide side chains minimally impacts the macromolecule optical properties with $\Delta\lambda_{max} < 10$ nm. Variation of the bridging atom from Si in **PBTISi** to Ge in **PBTIGe** also has minimal impact on the macromolecule optical properties with $\Delta\lambda_{max}$ and $\Delta\lambda_{shoulder} < 5$ nm. The calculated E_g^{opt}'s from the polymer film absorption edges fall within a small range of 1.75−1.77 eV (Table 1). In comparison to the optical bandgap of **BTI**-based polymer **PBTISi-C8**, **TPD**-based polymer **PTPDSi-C8** has a slightly smaller bandgap of 1.73 eV; however, note that the absorption profile of **PTPDSi-C8**

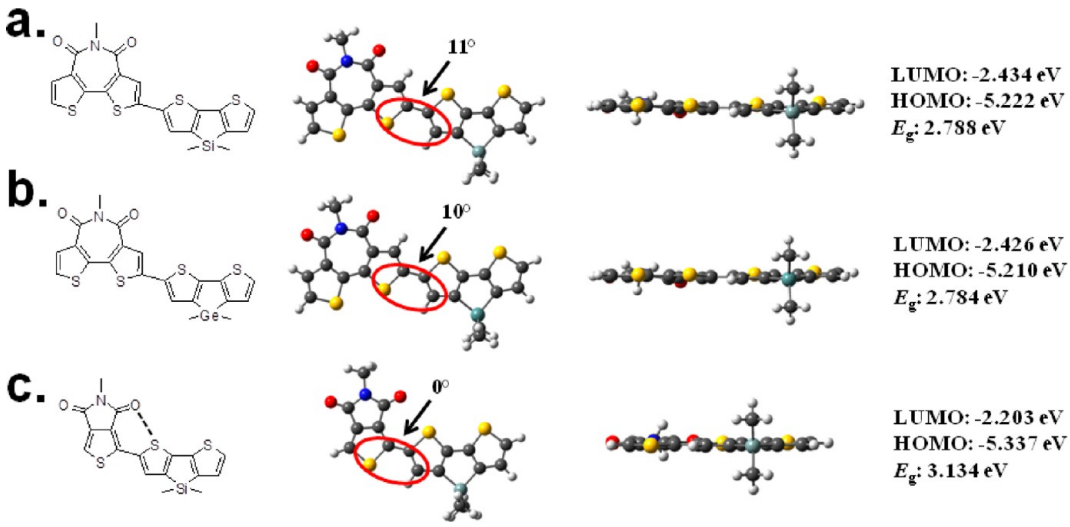

Figure 6. Chemical structures, optimized geometries, LUMO energies, HOMO energies, and E_g's for the polymer repeat units: (a) **PBTISi**, (b) **PBTIGe**, and (c) **PTPDSi**. Calculations were carried out at the DFT//B3LYP/6-31G** level; dihedral angles between the planes of donor block and acceptor block are indicated by red circles. Alkyl substitents are replaced here by methyl groups to simplify the calculations.

differs greatly from that of **PBTISi-C8** (Figure 5b). Thus, λ_{max} of **PTPDSi-C8** is red-shifted by 79 nm vs that of **PBTISi-C8** and also has significantly enhanced absorption in the red region, which may enhance exciton formation since the solar flux peaks here. Furthermore, the **PTPDSi-C8** absorption peak and shoulder are significantly sharper than those of **PBTISi-C8** both in solution and as thin film, suggesting a more ordered microstructure.[39]

Density functional theory (DFT) computation was also performed to obtain insights into the electronic structures and optical properties of the present **BTI**- and **TPD**-based polymers. The energy-minimized dihedral angle (Figure 6) is ~11° between the planes of **BTI** block and dithienosilole block in each repeating unit of **PBTISi**, and the dihedral angle is ~10° between planes of the **BTI** and dithienogermole blocks in each repeat unit of **PBTIGe**. In contrast, the computed dihedral angle is 0 °C between the planes of the **TPD** and dithienosilole blocks in each repeating unit of **PTPDSi** due to the intramolecular (thienyl)S···O(carbonyl) attractive interaction.[33,40,41] In fact, the computed (thienyl)S···O(carbonyl) distance in the **PTPDSi** repeat units is only 3.03 Å, which is significantly smaller than the sum of S and O van der Waals radii (3.32 Å). The slight backbone torsion in the **BTI**-based polymers accounts for their larger bandgaps and weaker absorption in the red region vs those of the **TPD**-based analogues. Note that, although backbone torsion results in a larger bandgap, it may promote larger V_{oc}'s, as seen in poly(alkylthiophene), PSCs.[42] The slight backbone torsion may reduce interchain π–π interactions, and hence affords useful solubilities for the present **BTI**-based polymers, although they contain fused **BTI** and **DTS/DTG** repeat units. For example, by employing the same side chains as those of **PTPDSi-C8**, **PBTISi-C8** still exhibits appreciable solubility at room temperature. Note also that the calculated E_g of the **PTPDSi** repeat unit (3.134 eV) is ~0.35 eV larger than those of **PBTISi** (2.788 eV) and **PBTIGe** (2.784 eV) due to the decreased conjugation length, i.e. three thiophene vs four thiophene units. As backbones are extended, this effect typically attenuates in conjugated polymers. For example, the calculated E_g of the **TPDSi** trimer (2.23 eV; Figure S2 in SI) is only ~0.13 eV larger than that of the **BTISi** trimer (2.10 eV; Figure S2 in SI).

Polymer Electrochemical Properties. The electrochemistry of the **BTI**-based polymers was investigated as thin films using cyclic voltammetry (CV). The ferrocene/ferrocenium (Fc/Fc^+) redox couple was used as standard, which was assigned an absolute energy of −4.80 eV vs vacuum.[43] The cyclic voltammograms of the **BTI**-based polymers are shown in Figure 7, and relevant data are collected in Table 1. On the basis of the

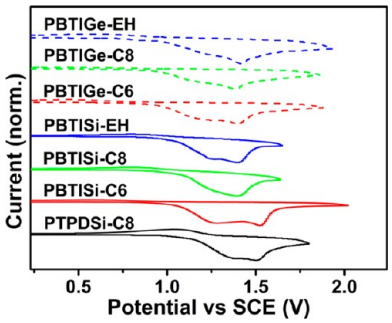

Figure 7. Cyclic voltammograms of **PBTISi** and **PBTIGe** polymer thin films measured in 0.1 M $(n\text{-Bu})_4N^+PF6^-$ acetonitrile electrolyte solution at scan rate of 50 mV/s (the Fc/Fc^+ redox couple is used as an standard). **PTPDSi-C8** is shown for comparison.

oxidation onsets, the estimated HOMO energies are −5.45 eV, −5.43 eV, −5.42 eV, −5.39, −5.38 eV, and −5.38 eV for **PBTISi-C6**, **PBTISi-C8**, **PBTISi-EH**, **PBTIGe-C6**, **PBTIGe-C8**, and **PBTIGe-EH**, respectively. Change of the donor units from dithienosilole to dithienogermole leads to destabilization of the HOMO levels by ~0.05 eV, which is in agreement with theoretical calculations on silole and germole oligomers[44a] and recent experiment results on the **TPD**-based analogues.[9a,44b] The cyclic voltammograms of **PTPDSi-C8** films were measured under identical conditions, and the oxidation potential was found to be 0.09 eV greater than that of **PBTISi-C8**, which translates to a 0.09 eV lower HOMO level for the latter polymer (−5.52 eV). Note that the measured HOMO energy levels are in good agreement with the DFT computational results (Figure 6) and the lower-lying HOMO of **PTPDSi-C8** correlates well with the greater density of electron-withdrawing imide groups vs **PBTISi-**

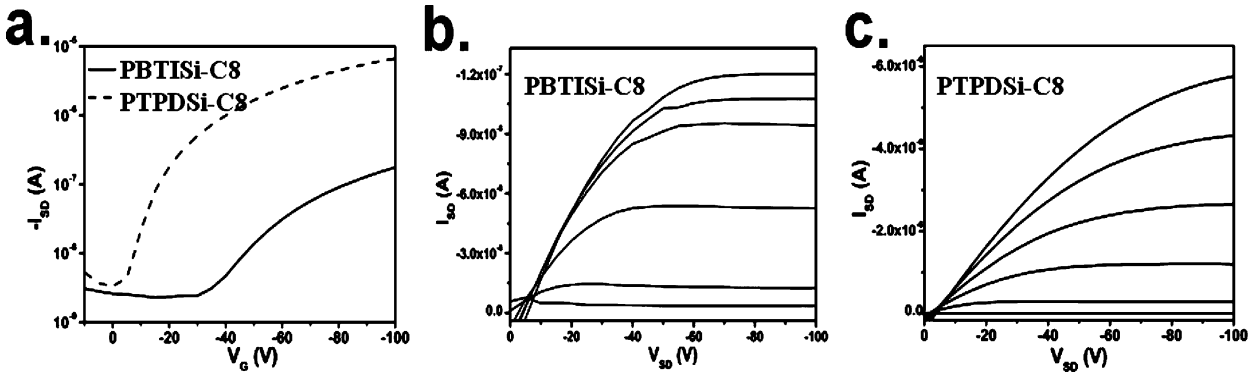

Figure 8. (a) Transfer characteristics for **PBTISi-C8**- and **PTPDSi-C8**-based bottom-gate/top-contact OTFTs. Output characteristics for (b) **PBTISi-C8**- and (c) **PTPDSi-C8**-based bottom-gate/top-contact OTFTs.

Table 2. Summary of Polymer Charge Transport and Optimized Photovoltaic Response Properties of BTI-Based Polymers PBTISi and PBTIGe in Inverted Bulk-Heterojunction Solar Cells; Optimized PTPDSi-C8 Solar Cell Performance is listed for Comparison

polymer	μ_h (cm^2/(V s))	D:A	solvent	solvent:DIO	thickness (nm)	V_{oc} (V)	J_{sc} (mA/cm^2)	J_{sc} (calc) (mA/cm^2)	FF (%)	PCE (%)
PBTISi-C6	2.06×10^{-4}	1:1	DCB	98:2	110	0.825	12.59	12.40	60.6	6.29
PBTISi-C8	1.08×10^{-4}	1:1	DCB	98:2	120	0.803	12.81	12.79	62.3	6.41
PBTISi-EH	0.85×10^{-4}	1:1	DCB	98:2	120	0.834	12.50	12.67	53.1	5.54
PBTIGe-C6	1.66×10^{-4}	1:1	DCB	97:3	110	0.774	12.30	11.96	50.2	4.77
PBTIGe-C8	1.42×10^{-4}	1:1.5	DCB	97:3	110	0.745	12.17	11.62	47.2	4.32
PBTIGe-EH	0.69×10^{-4}	1:1	DCB	97:3	110	0.769	10.09	9.97	46.7	3.62
PTPDSi-C8	2.61×10^{-3}	1:2	CB	97:3	90	0.885	11.90	11.80	64.9	6.83

C8. These results indicate that the strong electron-withdrawing capacity of the imide group is the dominant factor determining the polymer HOMO energetics. The higher imide group density in **PTPDSi-C8** yields a lower-lying HOMO than in **PBTISi-C8**, although **PBTISi-C8** has a higher degree of backbone torsion which can also depress the HOMO.[42] All of the present **BTI**-based polymers show well-defined oxidations; however, no reductive peaks are observed, which is different from the **TPD** polymer analogues.[38c] The LUMO energies compiled in Table 1 are derived by subtracting the optical bandgaps from the electrochemical oxidation data. The LUMO levels of the **BTI**-based polymers are in the range of −3.62 to −3.70 eV, yielding LUMO−LUMO offsets with the $PC_{71}BM$ acceptor of >0.3 eV, which should ensure efficient exciton dissociation.[13]

Organic Thin-Film Transistors. The charge transport properties of the present **BTI**-based polymers and **PTPDSi-C8** were investigated by fabricating organic thin-film transistors (OTFTs, see Supporting Information). The polymer films were deposited onto octadecyltrichlorosilane (OTS)-modified Si/SiO_2 substrates. All devices employed bottom-gate/top-contact configurations, and all polymers exhibited typical hole-transport properties (Figures 8 and S5 [SI]; Table 2), yielding mobilities of 2.06×10^{-4} cm^2/(V s), 1.08×10^{-4} cm^2/(V s), 0.85×10^{-4} cm^2/(V s), 1.66×10^{-4} cm^2/(V s), 1.42×10^{-4} cm^2/(V s), 0.69×10^{-4} cm^2/(V s), and 2.6×10^{-3} cm^2/(V s) (Table 2) for **PBTISi-C6**, **PBTISi-C8**, **PBTISi-EH**, **PBTIGe-C6**, **PBTIGe-C8**, **PBTIGe-EH**, and **PTPDSi-C8** respectively. The modest hole mobilities of the present polymers are in agreement with the low degree of order revealed by the DSC (Figure S1 in SI) and X-ray diffraction (XRD, Figure S4 in SI) data on the polymer films. Grazing incidence wide-angle X-ray scattering (GIWAXS), which is capable of characterizing partially ordered thin film materials, was then used to investigate the film microstructure and polymer chain packing orientation (Figure 9). Although Si/SiO_2 surface OTS-modification can promote π-polymers to adopt edge-on

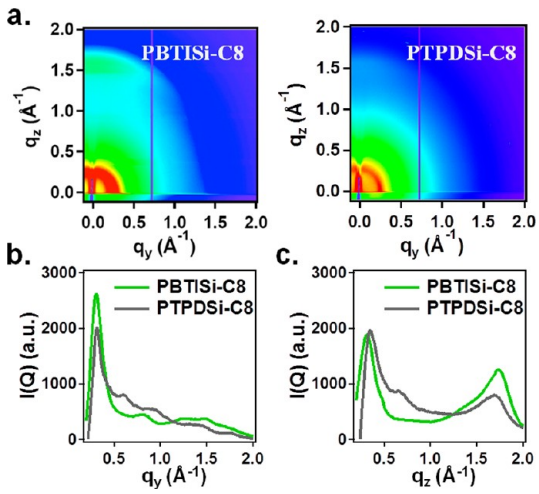

Figure 9. (a) Two-dimensional (2D) grazing incidence wide-angle X-ray scattering (GIWAXS) image of **PBTISi-C8** and **PTPDSi-C8**. (b) in-plane linecuts of 2D GIWAXS and (c) out-of-plane linecuts of 2D GIWAXS.

alignment, it was found that all of the present polymers exhibit predominantly face-on alignment, with a wide variation in the angle of face-on alignment as evidenced by the broad peak near q_z = 1.7 Å^{-1}, which differs greatly from the dominant edge-on orientation in typical crystalline polymer semiconductors,[42c,45] and therefore explains the low carrier mobility in the present OTFTs. In comparison to **PBTISi-C8**, **PTPDSi-C8** (Figure 9a) shows weaker out-of-plane diffraction arising from the 010 peak, which corresponds to the π−π stacking of polymer backbone. The derived π−π stacking distance of **PBTISi-C8** is 3.5 Å (Figure 9c); this compact π−π stacking is also observed in **BTI**-based small molecules.[31] The π−π stacking distance of **PTPDSi-C8** is 3.7 Å (Figure 9c), larger than that of **PBTISi-C8**. However, the

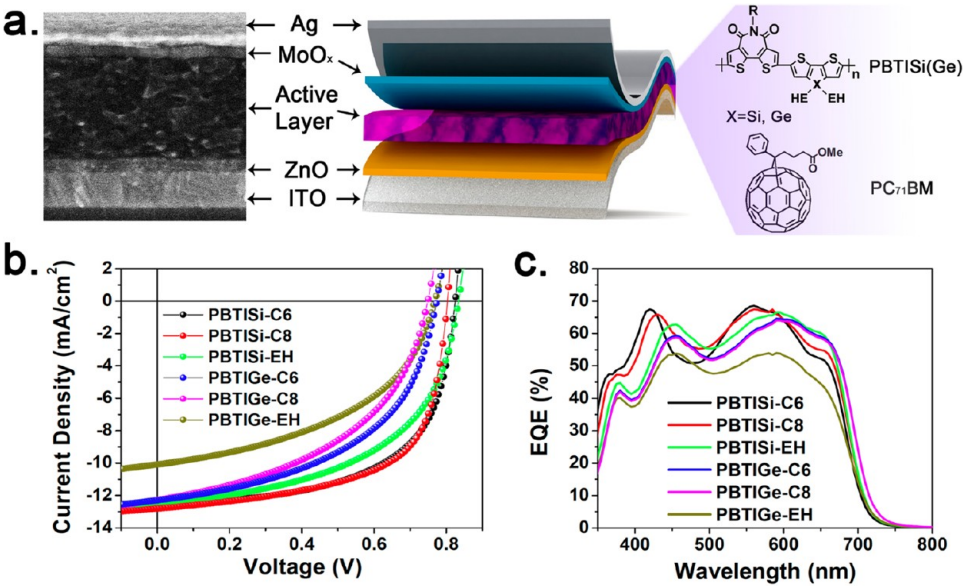

Figure 10. Inverted PSC device structure and performance: (a) SEM cross-sectional image of a **PBTISi-C8**:$PC_{71}BM$ (1:1) device fabricated with DCB:DIO (98:2 v/v) as the solvent; (b) illuminated $J-V$ characteristics of optimized **PBTISi** and **PBTIGe**-based PSCs; (c) external quantum efficiency of best-performing PSCs.

in-plane linecuts (Figure 9b) indicate that **PTPDSi-C8** has a higher degree of diffraction from lamellar stacking (100, 200, 300,....) than does **PBTISi-C8**, which could be induced by the higher degree of backbone coplanarity in **PTPDSi-C8**. The smaller $\pi-\pi$ stacking is likely to decrease the energetic barrier for intermolecular charge hopping; however, due to the face-on polymer backbone orientation, the $\pi-\pi$ stacking direction (perpendicular to substrate) is not the charge transport direction in OTFTs, which is parallel to the Si/SiO_2 substrate.

In summary, the enhanced lamellar stacking and higher degree of structural coplanarity in **PTPDSi-C8** leads to a one order of magnitude greater OTFT mobility than that in **PBTISi-C8**, although **PBTISi-C8** has more ordered and metrically closer $\pi-\pi$ stacking. The enhanced OTFT performance of **TPD**-based polymers[40] vs analogous **BTI**-based polymers[35] has also been reported in crystalline polymers. In comparison to the **PBTISi** polymer series, the **PBTIGe** polymer series typically shows weaker diffraction from $\pi-\pi$ stacking and lower intensity from lamellar stacking (Figure S10 in SI), resulting in lower charge carrier mobility. Note that the polymers **PBTISi-EH** and **PBTIGe-EH**, having branched *N*-substituents, exhibit mobilities lower than those of the corresponding analogues having linear *N*-substituents (Table 2), which may be attributed to the slightly larger $\pi-\pi$ stacking distance.[29,46]

Bulk-Heterojunction Photovoltaic Cells. The photovoltaic performance of the present **BTI**-based polymers was investigated by fabricating inverted bulk heterojunction (BHJ) solar cells having an ITO/ZnO/polymer:$PC_{71}BM$/MoOx/Ag architecture[8b] (Figure 10a, see SI for device fabrication details). Among the challenges facing current-generation PSCs,[1d,e,47] performance degradation when exposed to ambient air limits implementation on a large scale.[48] The inverted cell architecture minimizes environmental oxidation of low work function cathodes and eliminates the acidic PEDOT:PSS corrosion of ITO[49] in conventional cell architectures, and therefore enhances PSC durability. In the present work, the cathode interfacial layer, ZnO, was fabricated by sol–gel techniques,[8a] whereas the MoO_x anode interfacial layer was vacuum-deposited. $PC_{71}BM$ was chosen as the BHJ electron acceptor since it has increased optical absorption in the visible region vs [6,6]-phenyl-C_{61}-butyric acid methyl ester ($PC_{61}BM$). The morphology of the polymer/fullerene blend active layer plays a critical role in device performance,[5b] and the active layer should not only achieve nanoscale phase separation to maximize the exciton dissociation at the polymer/fullerene interface but also provide continuous interpenetrating donor/acceptor network for efficient charge carrier transport/collection at the respective electrodes.[12a]

For PSC device fabrication, chlorobenzene (CB) and *o*-dichlorobenzene (DCB) were chosen as processing solvents due to their good solvation properties and low evaporation rates, which allows time for polymer chain organization into an optimal BHJ film microstructure. Polymer/$PC_{71}BM$ blend ratios, spinning rates (film thickness), and processing additive concentrations were systematically investigated. Figure 10b shows the current–voltage ($J-V$) characteristics of optimized PSCs, and relevant photovoltaic data are collected in Table 2. All of the **BTI**-based polymers exhibit promising device performance with $J_{sc} \geq 10$ mA/cm^2, $V_{oc} \geq 0.75$ V, and PCEs typically >4%. The external quantum efficiency (EQE) integration vs an AM1.5 reference spectrum yields J_{sc}'s with ±5% of those acquired from the $J-V$ data (Table 2), showing good internal consistency. The best device performance is found for **PBTISi-C8**-based solar cells with a $J_{sc} = 12.81$ mA/cm^2, $V_{oc} = 0.803$ V, FF = 62.3%, and PCE = 6.41%. Note that the **PBTISi-C6**-based solar cells exhibit comparable PCEs (~6.3%). Polymers with branched *N*-2-ethylhexyl chains on the copolymer backbone exhibit inferior PCEs vs the polymers with linear chains, which can be attributed to the lower mobility, hence smaller J_{sc}'s and/or FFs.

The present dithienosilole-based **PBTISi** polymers generally exhibit enhanced PSC performance vs the analogous dithienogermole-based **PBTIGe** polymers, due principally to the higher V_{oc}'s and greater FFs. The lower V_{oc}'s of the **PBTIGe**-based solar cells are in good agreement with the electrochemical measurements (Table 1), and similar trends have been observed in other dithienogermole-based copolymers.[9a,38a,c,50] In contrast to the

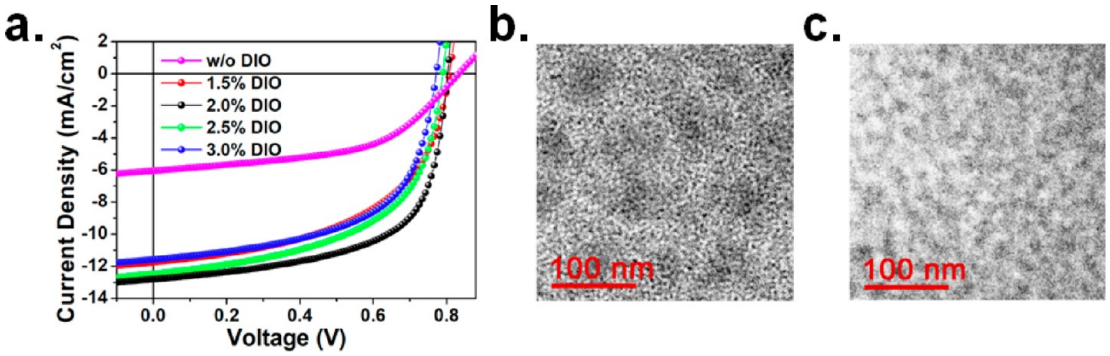

Figure 11. (a) Device performance of **PBTISi-C8**:$PC_{71}BM$ (1:1) inverted polymer solar cells fabricated using varying DIO concentrations; (b) TEM images of **PBTISi-C8**:$PC_{71}BM$ (1:1) without DIO, and (c) TEM images of **PBTISi-C8**:$PC_{71}BM$ (1:1) with DIO (DCB:DIO = 98:2; v/v as the solvent).

present **BTI**-based polymers, the dithienogermole-based **PTPDGe-C8** polymers achieve greater PCEs than the analogous dithienosilole-based **PTPDSi-C8** polymers in inverted solar cells.[9a] A plausible reason for the lower **PBTIGe** series performance vs the **PBTISi** series here is the lower M_n's of the **PBTIGe** series (Table 1). Lower M_n polymers typically exhibit inferior PSC performance as exemplified by **PTPDGe-C8** polymers[9a,S0] and others.[17e,30]

It is also known that processing additives,[5b] such as diiodooctane (DIO), can dramatically enhance device performance in **BTI**-based polymer solar cells. In the present study, the **PBTISi-C8** PCE is increased from 2.67% to 6.41% (Figure 11a) on film processing with 2% DIO. The greatly increased solar cell performance using this processing additive reflects nanoscale phase separation and increased BHJ film crystallinity (Figure 14c), which will be discussed in detail in the following film microstructure section.

PTPDSi-C8-based inverted solar cells were also fabricated, and optimized device performance data are included in Table 2, and compared to the **PBTISi-C8**-based devices. After extensive optimization, the **PTPDSi-C8**-based inverted solar cells achieve V_{oc} = 0.885 V, J_{sc} = 11.90 mA/cm^2, FF = 64.9%, and PCE = 6.83% (Figure 12a), which is perhaps slightly higher than the PCEs

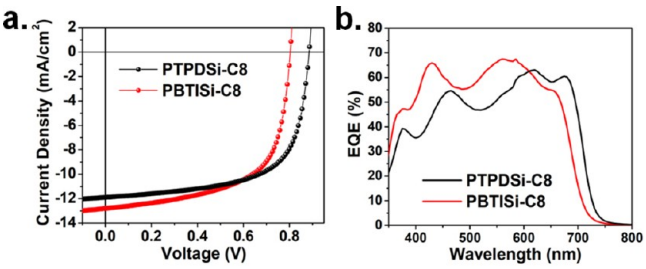

Figure 12. (a) Illuminated J−V characteristics and (b) external quantum efficiency spectra of optimized **PBTISi-C8** and **PTPDSi-C8**-based solar cells.

reported by Reynolds et al. in the same device structure (~6.6%).[9a] On the basis of the external quantum efficiency spectra of both cells (Figure 12b), the **PTPDSi-C8**-based inverted cells have greater absorption in the red region; however, the measured and calculated J_{sc}'s for the **PBTISi-C8** cells are about 1 mA/cm^2 larger than those of **PTPDSi-C8** (Figure 12a), which could be due to the more ordered, closer π−π stacking of **PBTISi-C8** vs that of **PTPDSi-C8** (Figures 9a and 14a). From the J−V characteristics, the enhanced device performance of the **PTPDSi-C8**-based PSCs is due primarily to the increase in V_{oc} by ~0.08 V, in good agreement with the electrochemical measurements on **PTPDSi-C8** (vide supra).

Film Morphology and Microstructure. To better understand the PSC performance of the present materials, AFM and TEM were employed to investigate the polymer/$PC_{71}BM$ blend microstructures. For the **PBTISi-C8**/$PC_{71}BM$ blend films processed without DIO, it can be seen that the $PC_{71}BM$-rich domains (Figure 11b, darker phase) with domain sizes of ~40−60 nm are embedded in the **PBTISi-C8**/$PC_{71}BM$ blend. This morphology is expected to result in inefficient exciton dissociation and lacks the bicontinuous interpenetrating pathways necessary for the charge carriers to reach their respective electrodes. Therefore, V_{oc} = 0.838 V, J_{sc} = 6.06 mA/cm^2, FF = 52.6%, and moderate PCE = 2.67% are obtained for cells fabricated under these conditions. In marked contrast, after optimization with 2% DIO as the processing additive, nanoscale phase separation with domain sizes of ~20 nm, which is approximately twice the typical exciton diffusion length,[12a] as well as a bicontinuous interpenetrating network, are clearly visible (Figure 11c). Note that PSCs fabricated/processed under these conditions achieve a greatly enhanced V_{oc} = 0.803 V, J_{sc} = 12.81 mA/cm^2, FF = 62.3%, and a good PCE = 6.41%. Indeed, using DIO as the processing additive enhances the device performance[5a,S1a] for all these **BTI**-based polymer solar cells (Tables 2 and S1 [SI]), Figure 13 shows AFM surface topographic and TEM images of **PBTISi** and **PBTIGe** blends fabricated under the conditions yielding the optimum PSC performance. Using the DIO processing additive, the AFM and

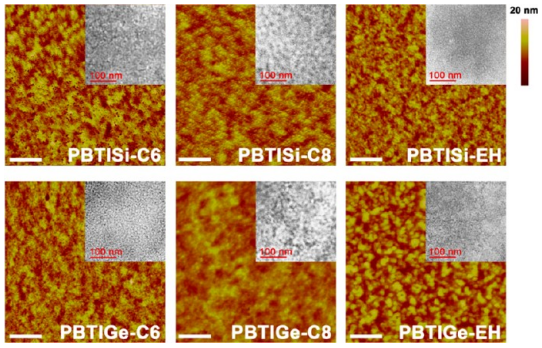

Figure 13. AFM topographical and TEM (insets) images of the indicated polymer/$PC_{71}BM$ blend films fabricated under conditions which yield the best-performing solar cells. AFM scale bars are 1 μm.

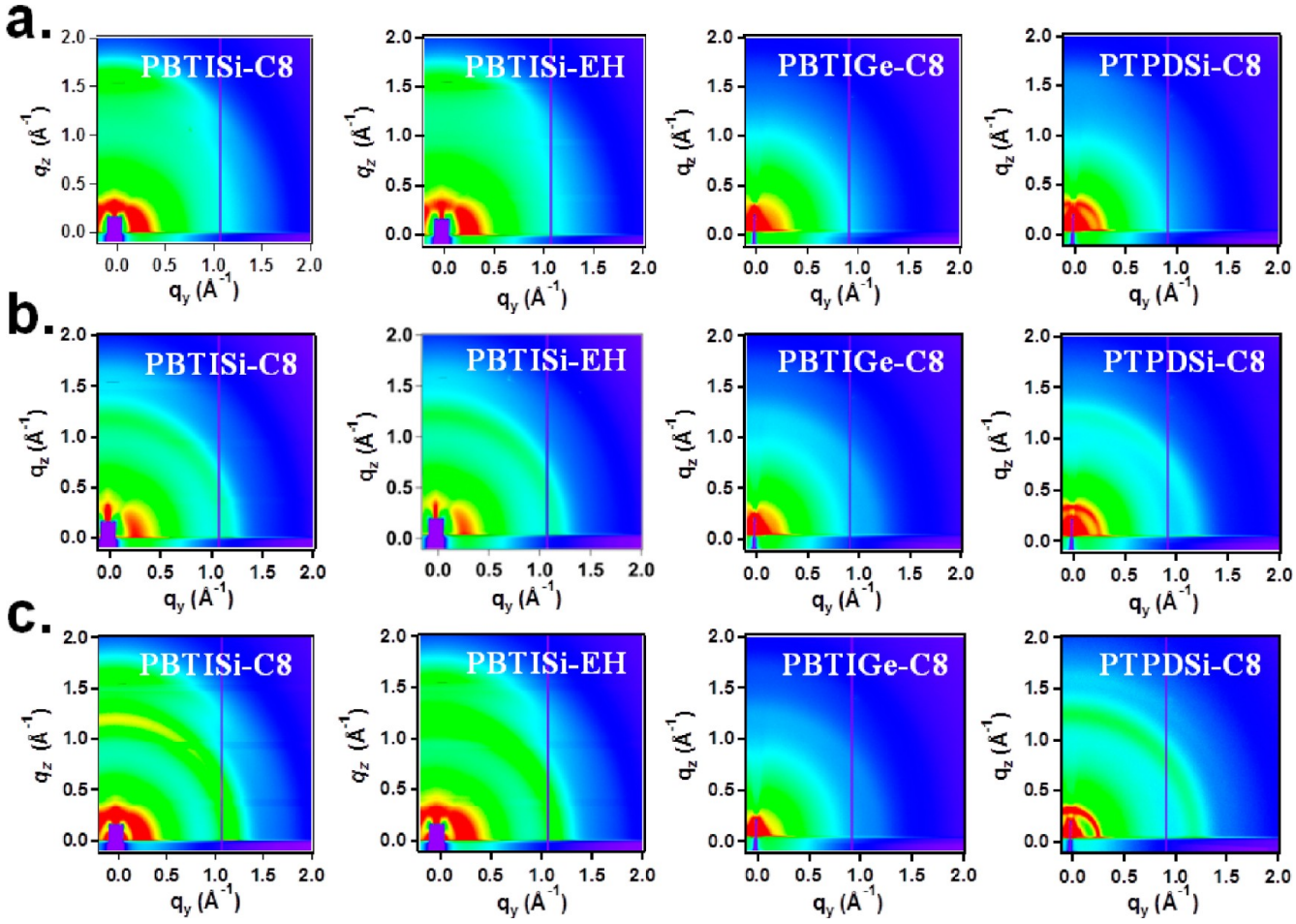

Figure 14. (a) Two-dimensional grazing incidence wide-angle X-ray scattering (GIWAXS) images of neat polymer films; (b) polymer:$PC_{71}BM$ blend films without DIO; and (c) polymer:$PC_{71}BM$ (1:1) blend films with DIO as the processing additive. The films are deposited on a ZnO-coated ITO substrate and the polymer/$PC_{71}BM$ ratios and DIO percentages are those yielding the best-performing solar cells.

TEM images of all specimens exhibit well-defined nanoscale phase separations and interpenetrating networks, which is requisite for efficient exciton dissociation at the polymer/$PC_{71}BM$ interfaces and efficient charge carrier transport to the electrodes, therefore optimal device performance.[5a,12a]

To further understand the device performance, GIWAXS was used to investigate the influence of the different *N*-alkyl substituents, bridging atoms (Si vs Ge), and acceptor units (**BTI** vs **TPD**) on polymer/$PC_{71}BM$ BHJ blend morphology. Neat polymer films without $PC_{71}BM$ were also characterized to study the evolution of film microstructure and chain orientation. Figure 14 shows scattering images for **PBTISi-C8**, **PBTISi-EH**, **PBTIGe-C8**, and **PTPDSi-C8** neat and BHJ blend films fabricated without and with diiodooctane (DIO). For the neat BHJ films deposited on ZnO, all polymers show dominant π-face-on polymer backbone orientation, similar to the neat films on OTS-modified substrates, which is the optimal orientation for charge extraction.[51b] Therefore, surface energy variations exert minimal impact on the alignment of these amorphous/low crystallinity polymers. Compared to the **PBTIGe** polymer series, the **PBTISi** polymer series exhibits a greater degree of ordering, both in lamellar and in $\pi-\pi$ stacking (Figures 14 and S11). Note that polymers having branched *N*-2-ethylhexyl substituents have slightly greater $\pi-\pi$ stacking distances vs the polymers having linear *N*-alkyl substituents, for example, 3.5 Å in **PBTISi-C8** vs 3.6 Å in **PBTISi-EH**. In comparison to **PBTISi-C8**, **PTPDSi-C8** exhibits a higher regularity of lamellar stacking as well as closer interchain stacking distances than in **PTPDSi-C8** (20.1 Å vs 21.8 Å in in **PBTISi-C8**).

Compared to the neat polymer films, the $\pi-\pi$ stacking in all the polymer:$PC_{71}BM$ blend films is disrupted (Figure 14b), while an isotropic ring feature (q = 1.4 Å^{-1}; d = 4.5 Å) in the 2D GIWAXS images corresponding to the $PC_{71}BM$ feature emerges.[52] After adding DIO, the diffraction intensity from the $\pi-\pi$ stacking is regained due to increased ordering of the molecular packing in the films, which is accompanied by a dramatic enhancement in performance for the optimized solar cells. In comparison to the **PBTISi-EH** blend films, the **PBTISi-C8** blend films exhibit more intense diffraction features at higher q values from the $\pi-\pi$ stacking (Figures 14c and Figure S11 [SI]), due to better stacking with shorter interchain spacing, similar to the situation in the neat polymer films. According to our previous results,[51b] such morphology should promote charge transport and lead to higher J_{sc} and FF in the **PBTISi-C8**-based cells. Similarly, the BJH films of **PBTISi-C8** with greater intensity in the $\pi-\pi$ stacking Bragg peak are more ordered than those of **PBTIGe-C8** and also exhibit higher J_{sc} and FF in the corresponding solar cells (Table 2). The in-plane GIWAXS linecuts show that **PTPDSi-C8** has a high degree of lamellar stacking (Figure S11c in SI); however, the out-of-plane linecuts (Figure S11f in SI) reveal that **PBTISi-C8** also has more ordered and closer $\pi-\pi$ stacking. The higher degree of lamellar stacking

can be linked to the planarity and rigidity of the **PTPDSi-C8** polymer backbone due to the (carbonyl)O···S(thienyl) attractive interaction (Figure 6c), and this can enhance intramolecular charge transport, as well as intermolecular charge transport *parallel* to the ITO substrate. In contrast, the more ordered and closer $\pi-\pi$ stacking in **PBTISi-C8** is expected to enhance intermolecular charge transport *perpendicular* to the substrate, which may account for the slightly higher J_{sc} of **PBTISi-C8** vs that of **PTPDSi-C8** in the optimized PSCs. The enhanced device performance of the **PTPDSi-C8**-based PSCs is mainly due to the greater V_{oc}.

■ CONCLUSIONS

A series of bithiopheneimide (**BTI**)-based polymer semiconductors having appreciable molecular weights (>18 kDa) and good solubilities was synthesized via Stille coupling for implementation in BHJ polymer solar cells. Due to the electron-deficient characteristics of the **BTI** units, the polymers exhibit low bandgaps of 1.75−1.77 eV and low-lying HOMO levels of −5.38 to −5.45 eV. A change in the electron-rich co-units from dithienosilole to dithienogermole has negligible effect on the optical properties, but has a significant impact on the HOMO energies of the resultant polymer semiconductors, resulting in destabilization of the HOMO by ∼0.05 eV for **PBTIGe**. *N*-alkyl side chain modifications on the imide group greatly alter the polymer solubility/processability and the resulting film microstructure, with linear *N*-substituents affording slightly more compact packing, and therefore more efficient charge transport. The TFT mobility of **TPD**-based polymer **PTPDSi-C8** is found to be 10× greater than that of the **BTI**-based analogue **PBTISi-C8**, which can be attributed to the higher degree of macromolecular coplanarity enforced by the intramolecular (thienyl)-S···O(carbonyl) attractive interactions in **PTPDSi-C8**. Locating the imide group at the center of bithiophene eliminates this interaction in the **BTI**-based polymers, resulting in a ∼11° backbone torsion between the **BTI** and dithienosilole planes, a ∼0.02 eV larger bandgap, and less structured optical absorption profiles for **PBTISi-C8**. However, such backbone torsions could, in principle, be beneficial for **BTI**-based polymer solubility vs the comparably functionalized **TPD**-based polymers, and the backbone torsion also offers a potential strategy to raise the ionization potential, hence the open-circuit voltage. The **TPD**-based **PTPDSi-C8** polymer HOMO is found to be lowered by ∼0.09 eV vs that of the **BTI**-based analogue **PBTISi-C8**, indicating that the strong imide group electron-withdrawing capacity is the dominant factor governing the HOMO energy. Note that the higher imide group density in **PTPDSi-C8** lowers the HOMO vs **PBTISi-C8**, although **PBTISi-C8** has greater backbone torsion.

The PSC performance of the **BTI**-based polymers was investigated by fabricating inverted BHJ solar cells having a ITO/ZnO/polymer:$PC_{71}BM$/MoO_x/Ag architecture. After optimizations, the **BTI**-based polymers show promising device performance with PCEs typically ≥4% and open circuit voltages ≥0.75 eV. In comparison to dithienogermole-based polymers **PBTIGe**, the dithienosilole-based polymers **PBTISi** exhibit slightly increased V_{oc}'s, in good agreement with the HOMO energies derived from electrochemical measurements. Microstructural investigations indicate that the processing additive, 1,8-diiodooctane (DIO), substantially promotes nanoscale phase separation and interpenetrating network formation and also enhances blend film crystallinity. The highest PCE = 6.41% is achieved in **PBTISi-C8**-based BHJ solar cells, which is slightly lower than that of the **PTPDSi-C8**-based PSCs having PCE = 6.83% in the optimized inverted geometries. GIWAXS investigation of polymer films reveals that polymers with linear *N*-alkyl chains have more compact packing. Compared to the **PBTIGe** polymer series, the **PBTISi** polymer series exhibits a higher degree of ordering, both in lamellar and $\pi-\pi$ stacking. Note that **PTPDSi-C8** shows a higher degree of lamellar ordering, but weaker and less close $\pi-\pi$ stacking than in **PBTISi-C8**. The PCE enhancement of the **PTPDSi-C8**-based cells is attributed primarily to the greater V_{oc}'s arising from the low-lying HOMOs. These results indicate the **BTI**-based polymers are very promising for solar cell applications, and these studies provide significant insight regarding structure−property device performance correlations in **BTI**- and **TPD**-based polymer semiconductors, which should guide the further design of high-performance polymer semiconductors for thin-film transistor and solar cell applications.

■ ASSOCIATED CONTENT

Ⓢ Supporting Information

Synthesis and characterization of monomers and polymers, details of OTFT and solar cell fabrication, UV−vis spectra, DFT calculations, DSC curves, OFET data, *J*−*V* characteristics of polymer solar cells, film morphologies, and GIWAXS data. This material is available free of charge via the Internet at http://pubs.acs.org.

■ AUTHOR INFORMATION

Corresponding Author

ratner@chem.northwestern.edu (M.A.R.); lchen@anl.gov (L.X.C.); r-chang@northwestern.edu (R.P.H.C.); a-facchetti@northwestern.edu (A.F.); t-marks@northwestern.edu (T.J.M.)

Author Contributions

▽These authors contributed equally.

Notes

The authors declare no competing financial interest.

■ ACKNOWLEDGMENTS

This research is supported as part of the ANSER Center, an Energy Frontier Research Center funded by the U.S. Department of Energy, Office of Science, and Office of Basic Energy Sciences under Award Number DE-SC0001059, by Polyera Corp., and by AFOSR (FA9550-08-1-0331). We thank the NSF-MRSEC program through the Northwestern University Materials Research Science and Engineering Center for characterization facilities (DMR-1121262) and Institute for Sustainability and Energy at Northwestern (ISEN) for partial equipment funding. Use of the Advanced Photon Source was supported by the U. S. Department of Energy, Office of Science, Office of Basic Energy Sciences, under Contract No. DE-AC02-06CH11357. R.P.O. acknowledges funding from the European Community's Seventh Framework Programme through a Marie Curie International Fellowship (Grant Agreement 234808). J.T.L. thanks financial support by the MICINN of Spain (projects CTQ2009-10098) and the Junta de Andalucía (project PO9-4708).

■ REFERENCES

(1) (a) Krebs, F. C. *Sol. Energy Mater. Sol. Cells* **2009**, *93*, 394−412. (b) Krebs, F. C.; Gevorgyan, S. A.; Alstrup, J. *J. Mater. Chem.* **2009**, *19*, 5442−5451. (c) Krebs, F. C.; Nielsen, T. D.; Fyenbo, J.; Wadstrøm, M.; Pedersen, M. S. *Energy Environ. Sci.* **2010**, *3*, 512−525. (d) Azzopardi, B.; Emmott, C. J. M.; Urbina, A.; Krebs, F. C.; Mutale, J.; Nelson, J. *Energy*

Environ. Sci. **2011**, *4*, 3741−3753. (e) Espinosa, N.; Hösel, M.; Angmo, D.; Krebs, F. *Energy Environ. Sci.* **2012**, *5*, 5117−5132.
(2) Arias, A. C.; MacKenzie, J. D.; McCulloch, I.; Rivnay, J.; Salleo, A. *Chem. Rev.* **2010**, *110*, 3−24.
(3) (a) Thompson, B. C.; Fréchet, J. M. J. *Angew. Chem., Int. Ed.* **2008**, *47*, 58−77. (b) Cheng, Y.-J.; Yang, S.-H.; Hsu, C.-S. *Chem. Rev.* **2009**, *109*, 5868−5923. (c) Chen, J.; Cao, Y. *Acc. Chem. Res.* **2009**, *42*, 1709−1718. (d) Inganäs, O.; Zhang, F.; Andersson, M. R. *Acc. Chem. Res.* **2009**, *42*, 1731−1739. (e) Liang, Y.; Yu, L. *Acc. Chem. Res.* **2010**, *43*, 1227−1236. (f) Gendron, D.; Leclerc, M. *Energy Environ. Sci.* **2011**, *4*, 1225−1237. (g) Li, Y. *Acc. Chem. Res.* **2012**, *45*, 723−733.
(4) (a) He, Y.; Chen, H.-Y.; Hou, J.; Li, Y. *J. Am. Chem. Soc.* **2010**, *132*, 1377−1382. (b) Zhou, H.; Yang, L.; Stuart, A. C.; Price, S. C.; Liu, S.; You, W. *Angew. Chem., Int. Ed.* **2011**, *50*, 2995−2998.
(5) (a) Peet, J.; Kim, J. Y.; Coates, N. E.; Ma, W. L.; Moses, D.; Heeger, A. J.; Bazan, G. C. *Nat. Mater.* **2007**, *6*, 497−500. (b) Peet, J.; Heeger, A. J.; Bazan, G. C. *Acc. Chem. Res.* **2009**, *42*, 1700−1708. (c) Brabec, C. J.; Heeney, M.; McCulloch, I.; Nelson, J. *Chem. Soc. Rev.* **2011**, *40*, 1185−1199.
(6) (a) Irwin, M. D.; Buchholz, B.; Hains, A. W.; Chang, R. P. H.; Marks, T. J. *Proc. Natl. Acad. Sci. U.S.A.* **2008**, *105*, 2783−2787. (b) Murray, I. P.; Lou, S. J.; Cote, L. J.; Loser, S.; Kadleck, C. J.; Xu, T.; Szarko, J. M.; Rolczynski, B. S.; Johns, J. E.; Huang, J.; Yu, L.; Chen, L. X.; Marks, T. J.; Hersam, M. C. *J. Phys. Chem. Lett.* **2011**, 3006−3012. (c) He, Z.; Zhong, C.; Huang, X.; Wong, W.-Y.; Wu, H.; Chen, L.; Su, S.; Cao, Y. *Adv. Mater.* **2011**, *23*, 4636−4643.
(7) (a) Armstrong, N. R.; Veneman, P. A.; Ratcliff, E.; Placencia, D.; Brumbach, M. *Acc. Chem. Res.* **2009**, *42*, 1748−1757. (b) Hotchkiss, P. J.; Jones, S. C.; Paniagua, S. A.; Sharma, A.; Kippelen, B.; Armstrong, N. R.; Marder, S. R. *Acc. Chem. Res.* **2012**, *45*, 337−346.
(8) (a) Chou, C.-H.; Kwan, W. L.; Hong, Z.; Chen, L.-M.; Yang, Y. *Adv. Mater.* **2011**, *23*, 1282−1286. (b) Sun, Y. M.; Seo, J. H.; Takacs, C. J.; Seifter, J.; Heeger, A. J. *Adv. Mater.* **2011**, *23*, 1679−1683. (c) Hau, S. K.; Yip, H.-L.; Jen, A. K. Y. *Polym. Rev.* **2010**, *50*, 474−510.
(9) (a) Amb, C. M.; Chen, S.; Graham, K. R.; Subbiah, J.; Small, C. E.; So, F.; Reynolds, J. R. *J. Am. Chem. Soc.* **2011**, *133*, 10062−10065. (b) Small, C. E.; Chen, S.; Subbiah, J.; Amb, C. M.; Tsang, S. W.; Lai, T. H.; Reynolds, J. R.; So, F. *Nature Photonics* **2012**, *6*, 115−120.
(10) Li, X.; Choy, W. C. H.; Huo, L.; Xie, F.; Sha, W. E. I.; Ding, B.; Guo, X.; Li, Y.; Hou, J.; You, J.; Yang, Y. *Adv. Mater.* **2012**, *24*, 3046−3052.
(11) Service, R. F. *Science* **2011**, *332*, 293−293.
(12) (a) Coakley, K. M.; McGehee, M. D. *Chem. Mater.* **2004**, *16*, 4533−4542. (b) Boudreault, P.-L. T.; Najari, A.; Leclerc, M. *Chem. Mater.* **2011**, *23*, 456−469.
(13) Scharber, M. C.; Mühlbacher, D.; Koppe, M.; Denk, P.; Waldauf, C.; Heeger, A. J.; Brabec, C. J. *Adv. Mater.* **2006**, *18*, 789−794.
(14) Servaites, J. D.; Ratner, M. A.; Marks, T. J. *Energy Environ. Sci* **2011**, *4*, 4410−4422.
(15) (a) Zhou, H.; Yang, L.; You, W. *Macromolecules* **2012**, *45*, 607−632. (b) Facchetti, A. *Chem. Mater.* **2011**, *23*, 733−758. (c) Beaujuge, P. M.; Fréchet, J. M. J. *J. Am. Chem. Soc.* **2011**, *133*, 20009−20029.
(16) (a) Roncali, J. *Chem. Rev.* **1997**, *97*, 173−206. (b) Thompson, B. C.; Kim, Y.-G.; McCarley, T. D.; Reynolds, J. R. *J. Am. Chem. Soc.* **2006**, *128*, 12714−12725. (c) Usta, H.; Risko, C.; Wang, Z.; Huang, H.; Deliomeroglu, M. K.; Zhukhovitskiy, A.; Facchetti, A.; Marks, T. J. *J. Am. Chem. Soc.* **2009**, *131*, 5586−5608.
(17) (a) Zhang, M.; Tsao, H. N.; Pisula, W.; Yang, C.; Mishra, A. K.; Müllen, K. *J. Am. Chem. Soc.* **2007**, *129*, 3472−3473. (b) Tsao, H. N.; Cho, D. M.; Park, I.; Hansen, M. R.; Mavrinskiy, A.; Yoon, D. Y.; Graf, R.; Pisula, W.; Spiess, H. W.; Müllen, K. *J. Am. Chem. Soc.* **2011**, *133*, 2605−2612. (c) Zhu, Z.; Waller, D.; Gaudiana, R.; Morana, M.; Mühlbacher, D.; Scharber, M.; Brabec, C. *Macromolecules* **2007**, *40*, 1981−1986. (d) Beaujuge, P. M.; Tsao, H. N.; Hansen, M. R.; Amb, C. M.; Risko, C.; Subbiah, J.; Choudhury, K. R.; Mavrinskiy, A.; Pisula, W.; Brédas, J.-L.; So, F.; Müllen, K.; Reynolds, J. R. *J. Am. Chem. Soc.* **2012**, *134*, 8944−8957. (e) Coffin, R. C.; Peet, J.; Rogers, J.; Bazan, G. C. *Nature Chem.* **2009**, *1*, 657−661. (f) Park, S. H.; Roy, A.; Beaupre, S.; Cho, S.; Coates, N.; Moon, J. S.; Moses, D.; Leclerc, M.; Lee, K.; Heeger, A. J. *Nat. Photonics* **2009**, *3*, 297−303.
(18) Blouin, N.; Michaud, A.; Gendron, D.; Wakim, S.; Blair, E.; Neagu-Plesu, R.; Belletête, M.; Durocher, G.; Tao, Y.; Leclerc, M. *J. Am. Chem. Soc.* **2008**, *130*, 732−742.
(19) (a) Wang, M.; Hu, X.; Liu, P.; Li, W.; Gong, X.; Huang, F.; Cao, Y. *J. Am. Chem. Soc.* **2011**, *133*, 9638−9641. (b) Osaka, I.; Shimawaki, M.; Mori, H.; Doi, I.; Miyazaki, E.; Koganezawa, T.; Takimiya, K. *J. Am. Chem. Soc.* **2012**, *134*, 3498−3507.
(20) Zhou, H.; Yang, L.; Price, S. C.; Knight, K. J.; You, W. *Angew. Chem., Int. Ed.* **2010**, *49*, 7992−7995.
(21) (a) Wienk, M. M.; Turbiez, M.; Gilot, J.; Janssen, R. A. J. *Adv. Mater.* **2008**, *20*, 2556−2560. (b) Qu, S.; Tian, H. *Chem. Commun.* **2012**, *48*, 3039−3051. (c) Bronstein, H.; Chen, Z.; Ashraf, R. S.; Zhang, W.; Du, J.; Durrant, J. R.; Shakya Tuladhar, P.; Song, K.; Watkins, S. E.; Geerts, Y.; Wienk, M. M.; Janssen, R. A. J.; Anthopoulos, T.; Sirringhaus, H.; Heeney, M.; McCulloch, I. *J. Am. Chem. Soc.* **2011**, *133*, 3272−3275. (d) Dou, L.; Gao, J.; Richard, E.; You, J.; Chen, C.-C.; Cha, K. C.; He, Y.; Li, G.; Yang, Y. *J. Am. Chem. Soc.* **2012**, *134*, 10071−10079.
(22) (a) Mei, J.; Graham, K. R.; Stalder, R.; Reynolds, J. R. *Org. Lett.* **2010**, *12*, 660−663. (b) Stalder, R.; Mei, J.; Reynolds, J. R. *Macromolecules* **2010**, *43*, 8348−8352. (c) Wang, E.; Ma, Z.; Zhang, Z.; Vandewal, K.; Henriksson, P.; Inganäs, O.; Zhang, F.; Andersson, M. R. *J. Am. Chem. Soc.* **2011**, *133*, 14244−14247.
(23) Liang, Y.; Xu, Z.; Xia, J.; Tsai, S.-T.; Wu, Y.; Li, G.; Ray, C.; Yu, L. *Adv. Mater.* **2010**, *22*, E135−E138.
(24) (a) Xin, H.; Guo, X.; Kim, F. S.; Ren, G.; Watson, M. D.; Jenekhe, S. A. *J. Mater. Chem.* **2009**, *19*, 5303−5310. (b) Xin, H.; Guo, X.; Ren, G.; Watson, M. D.; Jenekhe, S. A. *Adv. Energy Mater* **2012**, *2*, 575−582.
(25) (a) Meng, H.; Wudl, F. *Macromolecules* **2001**, *34*, 1810−1816. (b) Braunecker, W. A.; Owczarczyk, Z. R.; Garcia, A.; Kopidakis, N.; Larsen, R. E.; Hammond, S. R.; Ginley, D. S.; Olson, D. C. *Chem. Mater.* **2012**, *24*, 1346−1356. (c) Douglas, J. D.; Griffini, G.; Holcombe, T. W.; Young, E. P.; Lee, O. P.; Chen, M. S.; Fréchet, J. M. J. *Macromolecules* **2012**, *45*, 4069−4074.
(26) (a) Zhan, X.; Facchetti, A.; Barlow, S.; Marks, T. J.; Ratner, M. A.; Wasielewski, M. R.; Marder, S. R. *Adv. Mater.* **2011**, *23*, 268−284. (b) Guo, X.; Kim, F. S.; Seger, M. J.; Jenekhe, S. A.; Watson, M. D. *Chem. Mater.* **2012**, *24*, 1434−1442.
(27) (a) Carsten, B.; Szarko, J. M.; Son, H. J.; Wang, W.; Lu, L.; He, F.; Rolczynski, B. S.; Lou, S. J.; Chen, L. X.; Yu, L. *J. Am. Chem. Soc.* **2011**, *133*, 20468−20475. (b) Carsten, B.; Szarko, J. M.; Lu, L.; Son, H. J.; He, F.; Botros, Y. Y.; Chen, L. X.; Yu, L. *Macromolecules* **2012**, *45*, 6390−6395.
(28) Carsten, B.; He, F.; Son, H. J.; Xu, T.; Yu, L. *Chem. Rev.* **2011**, *111*, 1493−1528.
(29) Guo, X.; Kim, F. S.; Jenekhe, S. A.; Watson, M. D. *J. Am. Chem. Soc.* **2009**, *131*, 7206−7207.
(30) Chu, T.-Y.; Lu, J.; Beaupré, S.; Zhang, Y.; Pouliot, J.-R.; Zhou, J.; Najari, A.; Leclerc, M.; Tao, Y. *Adv. Funct. Mater.* **2012**, *22*, 2345−2351.
(31) Letizia, J. A.; Salata, M. R.; Tribout, C. M.; Facchetti, A.; Ratner, M. A.; Marks, T. J. *J. Am. Chem. Soc.* **2008**, *130*, 9679−9694.
(32) (a) Najari, A.; Beaupre, S.; Berrouard, P.; Zou, Y.; Pouliot, J. R.; Lepage-Perusse, C.; Leclerc, M. *Adv. Funct. Mater.* **2011**, *21*, 718−728. (b) Li, Z.; Tsang, S. W.; Du, X.; Scoles, L.; Robertson, G.; Zhang, Y.; Toll, F.; Tao, Y.; Lu, J.; Ding, J. *Adv. Funct. Mater.* **2011**, *21*, 3331−3336.
(33) (a) Pomerantz, M. *Tetrahedron Lett.* **2003**, *44*, 1563−1565. (b) Berrouard, P.; Grenier, F.; Pouliot, J.-R.; Gagnon, E.; Tessier, C.; Leclerc, M. *Org. Lett.* **2011**, *13*, 38−41. (c) Huang, H.; Chen, Z.; Ortiz, R. P.; Newman, K.; Usta, H.; Lou, S.; Youn, J.; Noh, Y.-Y.; Baeg, K.-J.; Chen, L. X.; Facchetti, A.; Marks, T. *J. Am. Chem. Soc.* **2012**, *134*, 10966−10973.
(34) Guo, X.; Xin, H.; Kim, F. S.; Liyanage, A. D. T.; Jenekhe, S. A.; Watson, M. D. *Macromolecules* **2011**, *44*, 269−277.
(35) Guo, X.; Ortiz, R. P.; Zheng, Y.; Hu, Y.; Noh, Y. Y.; Baeg, K. J.; Facchetti, A.; Marks, T. J. *J. Am. Chem. Soc.* **2011**, *133*, 1405−1418.
(36) Hou, J.; Park, M.-H.; Zhang, S.; Yao, Y.; Chen, L.-M.; Li, J.-H.; Yang, Y. *Macromolecules* **2008**, *41*, 6012−6018.

(37) Zhou, N.; Guo, X.; Ortiz, R. P.; Li, S.; Zhang, S.; Chang, R. P. H.; Facchetti, A.; Marks, T. J. *Adv. Mater.* **2012**, *24*, 2242−2248.
(38) (a) Hou, J.; Chen, H.-Y.; Zhang, S.; Li, G.; Yang, Y. *J. Am. Chem. Soc.* **2008**, *130*, 16144−16145. (b) Chen, H.-Y.; Hou, J.; Hayden, A. E.; Yang, H.; Houk, K. N.; Yang, Y. *Adv. Mater.* **2010**, *22*, 371−375. (c) Chu, T. -Y.; Lu, J.; Beaupré, S.; Zhang, Y.; Pouliot, J. R.; Wakim, S.; Zhou, J.; Leclerc, M.; Li, Z.; Ding, J.; Tao, Y. *J. Am. Chem. Soc.* **2011**, *133*, 4250−4253. (d) Lu, G.; Usta, H.; Risko, C.; Wang, L.; Facchetti, A.; Ratner, M. A.; Marks, T. J. *J. Am. Chem. Soc.* **2008**, *130*, 7670−7685.
(39) (a) Halkyard, C. E.; Rampey, M. E.; Kloppenburg, L.; Studer-Martinez, S. L.; Bunz, U. H. F. *Macromolecules* **1998**, *31*, 8655−8659. (b) Kim, J.; Swager, T. M. *Nature* **2001**, *411*, 1030−1034.
(40) Guo, X.; Ortiz, R. P.; Zheng, Y.; Kim, M.-G.; Zhang, S.; Hu, Y.; Lu, G.; Facchetti, A.; Marks, T. J. *J. Am. Chem. Soc.* **2011**, *133*, 13685−13697.
(41) Hergué, N.; Mallet, C.; Savitha, G.; Allain, M.; Frère, P.; Roncali, J. *Org. Lett.* **2011**, *13*, 1762−1765.
(42) (a) Hou, J.; Chen, T.; Zhang, S.; Huo, L.; Sista, S.; Yang, Y. *Macromolecules* **2009**, *42*, 9217−9219. (b) Ko, S.; Verploegen, E.; Hong, S.; Mondal, R.; Hoke, E. T.; Toney, M. F.; McGehee, M. D.; Bao, Z. *J. Am. Chem. Soc.* **2011**, *133*, 16722−16725. (c) Ko, S.; Hoke, E. T.; Pandey, L.; Hong, S.; Mondal, R.; Risko, C.; Yi, Y.; Noriega, R.; McGehee, M. D.; Brédas, J.-L.; Salleo, A.; Bao, Z. *J. Am. Chem. Soc.* **2012**, *134*, 5222−5232.
(43) Pavlishchuk, V. V.; Addison, A. W. *Inorg. Chim. Acta* **2000**, *298*, 97−102.
(44) (a) Yamaguchi, S.; Itami, Y.; Tamao, K. *Organometallics* **1998**, *17*, 4910−4916. (b) Fei, Z.; Kim, Y.; Smith, J.; Domingo, E. B.; Stingelin, N.; McLachlan, M. A.; Song, K.; Anthopoulos, T. D.; Heeney, M. *Macromolecules* **2012**, *45*, 735−742.
(45) McCulloch, I.; Heeney, M.; Bailey, C.; Genevicius, K.; MacDonald, I.; Shkunov, M.; Sparrowe, D.; Tierney, S.; Wagner, R.; Zhang, W.; Chabinyc, M. L.; Kline, R. J.; McGehee, M. D.; Toney, M. F. *Nat. Mater.* **2006**, *5*, 328−333.
(46) Piliego, C.; Holcombe, T. W.; Douglas, J. D.; Woo, C. H.; Beaujuge, P. M.; Fréchet, J. M. J. *J. Am. Chem. Soc.* **2010**, *132*, 7595−7597.
(47) (a) Espinosa, N.; García-Valverde, R.; Urbina, A.; Lenzmann, F.; Manceau, M.; Angmo, D.; Krebs, F. C. *Sol. Energy Mater. Sol. Cells* **2012**, *97*, 3−13. (b) Andersen, T. R.; Larsen-Olsen, T. T.; Andreasen, B.; Böttiger, A. P. L.; Carlé, J. E.; Helgesen, M.; Bundgaard, E.; Norrman, K.; Andreasen, J. W.; Jørgensen, M.; Krebs, F. C. *ACS Nano* **2011**, *5*, 4188−4196. (c) Espinosa, N.; Garcia-Valverde, R.; Krebs, F. C. *Energy Environ. Sci.* **2011**, *4*, 1547−1557. (d) Krebs, F. C.; Tromholt, T.; Jorgensen, M. *Nanoscale* **2010**, *2*, 873−886. (e) Manceau, M.; Angmo, D.; Jorgensen, M.; Krebs, F. C. *Org. Electron.* **2011**, *12*, 566−574.
(48) (a) Norrman, K.; Madsen, M. V.; Gevorgyan, S. A.; Krebs, F. C. *J. Am. Chem. Soc.* **2010**, *132*, 16883−16892. (b) Jørgensen, M.; Norrman, K.; Gevorgyan, S. A.; Tromholt, T.; Andreasen, B.; Krebs, F. C. *Adv. Mater.* **2012**, *24*, 580−612.
(49) (a) Hains, A. W.; Ramanan, C.; Irwin, M. D.; Liu, J.; Wasielewski, M. R.; Marks, T. J. *ACS Appl. Mater. Interfaces* **2009**, *2*, 175−185. (b) Hains, A. W.; Liu, J.; Martinson, A. B. F.; Irwin, M. D.; Marks, T. J. *Adv. Funct. Mater.* **2010**, *20*, 595−606.
(50) Gendron, D.; Morin, P.-O.; Berrouard, P.; Allard, N.; Aïch, B. R.; Garon, C. N.; Tao, Y.; Leclerc, M. *Macromolecules* **2011**, *44*, 7188−7193.
(51) (a) Lou, S. J.; Szarko, J. M.; Xu, T.; Yu, L.; Marks, T. J.; Chen, L. X. *J. Am. Chem. Soc.* **2011**, *133*, 20661−20663. (b) Szarko, J. M.; Guo, J.; Liang, Y.; Lee, B.; Rolczynski, B. S.; Strzalka, J.; Xu, T.; Loser, S.; Marks, T. J.; Yu, L.; Chen, L. X. *Adv. Mater.* **2010**, *22*, 5468−5472.
(52) Woo, C. H.; Thompson, B. C.; Kim, B. J.; Toney, M. F.; Fréchet, J. M. J. *J. Am. Chem. Soc.* **2008**, *130*, 16324−16329.